Simultaneous position and mass determination of a nanoscale-thickness cantilever sensor in viscous fluids

Seongkyeol Hong, Deokman Kim, Junhong Park, and Jaesung Jang

Citation: Applied Physics Letters **106**, 063106 (2015); doi: 10.1063/1.4906613

View online: http://dx.doi.org/10.1063/1.4906613

View Table of Contents: http://scitation.aip.org/content/aip/journal/apl/106/6?ver=pdfcov

Published by the AIP Publishing

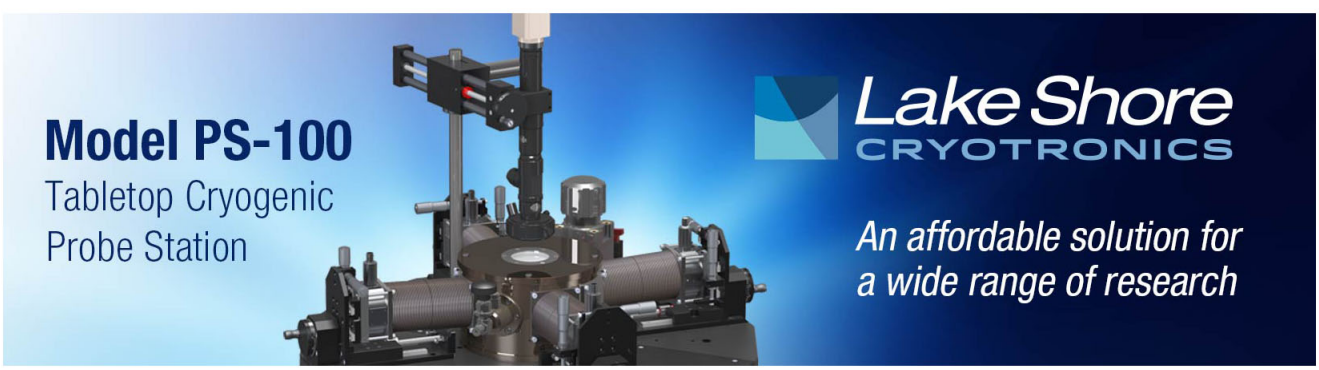

Simultaneous position and mass determination of a nanoscale-thickness cantilever sensor in viscous fluids

Seongkyeol Hong,[1,a)] Deokman Kim,[2,a)] Junhong Park,[2,b)] and Jaesung Jang[1,b)]
[1]*Department of Mechanical Engineering, Ulsan National Institute of Science and Technology (UNIST), Ulsan 689-798, South Korea*
[2]*School of Mechanical Engineering, Hanyang University, Seoul 133-791, South Korea*

(Received 15 October 2014; accepted 14 January 2015; published online 10 February 2015)

We report simultaneous determination of the mass and position of micro-beads attached to a nanoscale-thickness cantilever sensor by analyzing wave propagations along the cantilever while taking into account viscous and inertial loading due to a surrounding fluid. The fluid-structure interaction was identified by measuring the change in the wavenumber under different fluid conditions. The predicted positions and masses agreed with actual measurements. Even at large mass ratios (6%–21%) of the beads to the cantilever, this wave approach enabled accurate determination of the mass and position, demonstrating the potential for highly accurate cantilever sensing of particle-based bio-analytes such as bacteria. © *2015 AIP Publishing LLC*.
[http://dx.doi.org/10.1063/1.4906613]

In the last few decades, a large number of cantilever-based biosensors have been developed to detect proteins, deoxyribonucleic acids, cells, bacteria, and viruses for a variety of applications such as homeland security, clinical diagnostics, food safety analysis, and environmental monitoring.[1,2] These sensors generally measure either the changes in surface stress or resonant frequency shifts to find the masses of the target analytes.[1–3]

It is well known that the resonant frequency shift due to the attachment of a target analyte changes with its position on the cantilever sensor.[4] If it is not placed at the tip, its position needs to be determined to extract the actual mass from the measured frequency shift. Although it is critical to find both the position and the mass for ultrasensitive and highly accurate detection, only a few studies have been conducted. An approximate solution based on the Rayleigh-Ritz method has been developed for a vibrating cantilever with attached beads, and a perturbation technique has also been used to find the functional relationship between the frequency response and the mass at a particular position.[5–7] These methods are based on the assumption that the mass ratio of the attached beads to the cantilever is small enough not to change the vibration energy and the mode shape of the cantilever.

We previously presented the simultaneous measurement of the mass and position of micro-beads attached to commercially available micro-cantilevers.[8] The position of the beads was identified using their influence on the cantilever kinetic energy, and the bead mass was then obtained by analyzing the wave propagations. However, the viscous and inertial loading effects due to a surrounding fluid were neglected in this study. Therefore, this method has serious limitations on the use of nanoscale-thickness cantilevers even in gas media because the viscous effects due to a surrounding fluid increase significantly as the cantilever size decreases,[9] although the limit of detection (LOD) of a resonant cantilever sensor improves as the cantilever size decreases.[1,2]

In this paper, we present a modified technique to simultaneously detect the position and mass of micro-beads attached to a nanoscale-thickness cantilever by taking into account the viscous and inertial loading effects. The fluid-structure interaction between the surrounding fluid and the cantilever was estimated by measuring the change in the wavenumber. Moreover, the mass ratio of the attached beads to the cantilever was tested up to 6%–21%. These are quite large ratios compared to those used in the previous methods, and such large values have never been studied before. In fact, in the case of a large attached mass, the standing wave pattern changes considerably due to the mass discontinuity and fluid loading, resulting in changes in the mode shapes. If a nanoscale-thickness cantilever is used, as in the present study, these changes become more significant. Consequently, the assumption that the mode shapes do not change with the attached mass yields large identification inaccuracies. However, this assumption was not made in this study.

For a vibrating cantilever having a small thickness and width compared to the length, the effects of the shear deformation and rotary inertia are negligible compared to those of the bending deformation. In this case, the equation of motion for a cantilever immersed in a fluid is given by[10]

$$EI\frac{\partial^4 w(x,t)}{\partial x^4} + M_b\frac{\partial^2 w(x,t)}{\partial t^2} = F(x,t), \tag{1}$$

where E is Young's modulus, I is the moment of inertia, w is the deflection, x is the lengthwise coordinate along the base, M_b is mass per unit length of the cantilever, and F is the force induced by the fluid-structure interaction. The interaction force due to the fluid loading is given by[9,11]

$$F(x,\omega) = \frac{\pi}{4}\rho\omega^2 b^2\Gamma(\omega)w(x,\omega), \tag{2}$$

where ρ is the density of the fluid, ω is the radial frequency, b is the width, and $\Gamma(\omega)$ is the hydrodynamic function of the

[a)]S. Hong and D. Kim contributed equally to this work.
[b)]Authors to whom correspondence should be addressed. Electronic addresses: parkj@hanyang.ac.kr, Tel.: +82-2-2220-0424 and jjang@unist.ac.kr, Tel.: +82-52-217-2323.

cantilever. The hydrodynamic function can be expressed as $\Gamma(\omega) = \Gamma_r(\omega) + i\Gamma_i(\omega)$, where i is the imaginary number, assuming that the deflection of the cantilever has the form $w(x,t) = \text{Real}\{\hat{w}(x)e^{-i\omega t}\}$. The hydrodynamic function depends on the Reynolds number,[12] $\text{Re} = \rho\omega b^2/4\eta$, where η is the viscosity of the fluid. The hydrodynamic function for a rectangular cross-section cantilever, $\Gamma_{\text{rect}}(\omega)$, can be numerically calculated in the range of $\text{Re} \in [10^{-6}, 10^4]$ by using the theoretical solution derived for a circular cross-section cantilever and the correction function, Ω, in the following equation:[9]

$$\Gamma_{\text{rect}}(\omega) = \Omega(\omega)\Gamma_{\text{circ}}(\omega) = \Omega(\omega)\left[1 + \frac{4iK_1\left(-i\sqrt{i\text{Re}}\right)}{\sqrt{i\text{Re}}K_0\left(-i\sqrt{i\text{Re}}\right)}\right], \tag{3}$$

where K_0 and K_1 are the modified Bessel functions of the third kind, and the correction function is expressed as fractional polynomial functions of $\log_{10}\text{Re}$.[9]

Assuming harmonic vibration, the cantilever response can be expressed as

$$\hat{w}(x) = \hat{A}_1 \sin\hat{k}_b x + \hat{A}_2 \cos\hat{k}_b x + \hat{A}_3 e^{\hat{k}_b(x-L)} + \hat{A}_4 e^{-\hat{k}_b x}, \tag{4}$$

where $\hat{A}_j$ are the coefficients to be determined by boundary conditions, L is the cantilever length, and $\hat{k}_b$ is the wavenumber. The fluid-structure interaction has a relationship with the wavenumber, which is given by

$$\hat{k}_b = \{\omega^2(4M_b + \pi\rho b^2\Gamma_r - i\pi\rho b^2\Gamma_i)/4\hat{D}\}^{1/4}, \tag{5}$$

where $\hat{D}$ is the complex stiffness of the cantilever, and it is introduced to model both the vibration dissipation and the elasticity. Applying the boundary conditions, the vibration response can be computed. The transfer function between the input excitation and the resulting cantilever displacements can now be exactly determined by

$$\Lambda e^{i\phi} = \hat{w}(x_1)/w_0, \tag{6}$$

where x_1 is the measurement position, w_0 is the input deflection at the base, and Λ and ϕ are the amplitude and phase of the transfer function, respectively.[13,14] If the transfer function for a bare cantilever is measured, Eq. (6) is a function of the wavenumber, $\hat{k}_b$, and can be solved using the Newton-Raphson method. The detailed procedure for determining the mass and position is shown in Fig. 1.

Bead attachment also changes the vibration characteristics of the cantilever, and hence the wavenumber changes due to the mass discontinuity and mass increase. If the wavenumber is determined from the measured transfer function for a bead-attached cantilever in a fluid, the equivalent cantilever mass, M_b', can be obtained by

$$M_b' = \hat{k}_b{}^4\hat{D}/\omega^2 - \pi\rho b^2\Gamma_r/4 + i\pi\rho b^2\Gamma_i/4, \tag{7}$$

where the complex stiffness and the hydrodynamic function are obtained before the bead attachment. The imaginary component of the equivalent mass in Eq. (7) turned out to be negligibly small, and the effects of the mass attachment dominated

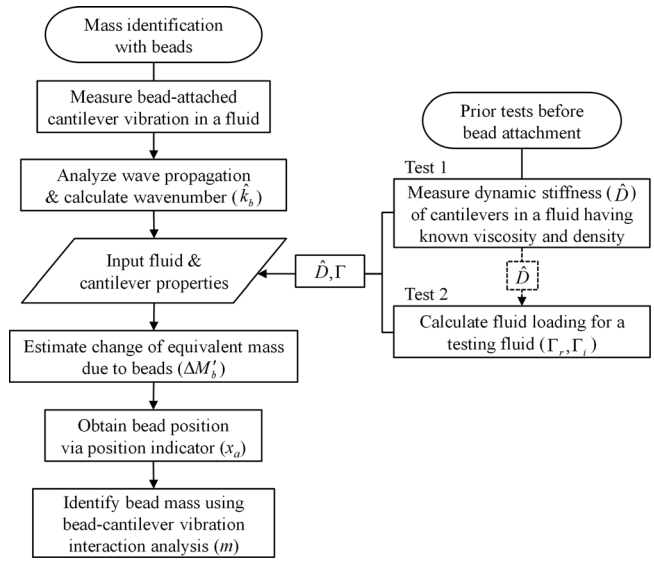

FIG. 1. The procedure of determining the mass attached to a nanoscale-thickness cantilever in a viscous fluid and its position using the vibration approach considering the fluid-structure interaction.

the real component. Therefore, the imaginary equivalent mass terms calculated from Eq. (7) were neglected.

The sensitivity of the equivalent mass to the bead position depends on the relative magnitude of the kinetic energy at the bead position compared to the average kinetic energy, and it is used to find the position indicator, *PI*, which is computed using the correlation as

$$PI(x) = \text{cov}(\Delta M_b', S)/\sqrt{\text{var}(\Delta M_b')\text{var}(S)}, \tag{8}$$

where $\Delta M_b' = M_b' - M_b$ and S is the sensitivity.[8] The maximum value of *PI* shows the bead position, x_a. The bead mass m can then be determined by analyzing the boundary condition at $x = x_a$, which is given by

$$EI\left[\frac{d\hat{w}_2(x_a)}{dx^3} - \frac{d\hat{w}_1(x_a)}{dx^3}\right] = m\omega^2\hat{w}_2(x_a), \tag{9}$$

where w_1 and w_2 are the cantilever responses for $x < x_a$ and $x \geq x_a$, respectively. As the bead position and wavenumber for the cantilever immersed in a fluid are pre-determined, the bead mass is determined from Eq. (9).

The fabrication of the nanoscale-thickness cantilevers was started using silicon-on-insulator wafers (SOI, P-type ⟨100⟩, Shanghai Simgui Technology, China). The cantilevers were patterned on the top silicon layer (nominal thickness: 200 nm) using reactive ion etching. After dicing a wafer into chips, about 35 μm of the bulk silicon below the buried oxide layer was isotropically etched by XeF_2 gas. The remaining buried oxide underneath the patterned cantilevers was removed by buffered oxide etching, and the photoresist on top of the cantilevers was removed to release the cantilevers. The cantilever chips were then piranha cleaned, mildly rinsed with deionized water, and dipped in deionized water for 1 h, followed by air-drying for 1 h. Commercially available thick cantilevers (TL-CONT, Nanosensors, Switzerland) were also used for comparison.

These cantilevers were fixed onto a PZT sheet (lead-zirconate-titanate; $10 \times 10 \times 0.5$ mm, Physik Instrumente Corporation,

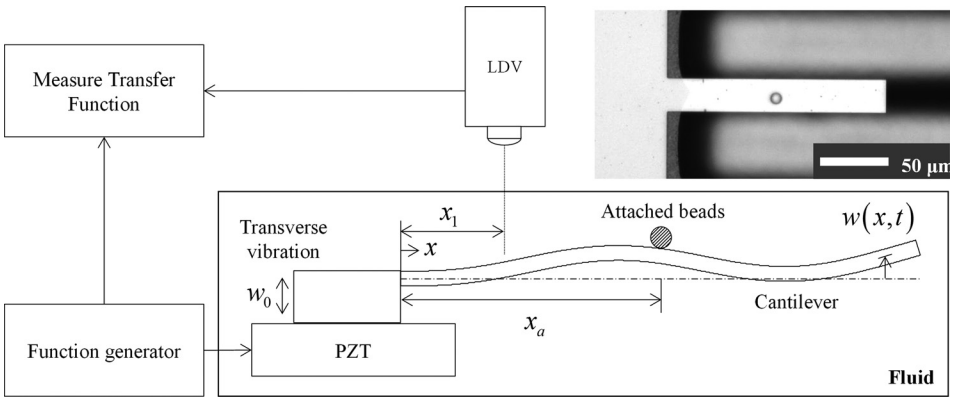

FIG. 2. A schematic of the experimental set-up, which consisted of a microfabricated nanoscale-thickness cantilever in a fluid chamber, a single-point laser Doppler vibrometer, a function generator, and a PZT. The vibration velocity of the cantilever was measured at $x = x_1$ via the laser Doppler vibrometer. The inset shows an image of a 7 μm polystyrene micro-bead attached to the nanoscale-thickness cantilever.

Germany) and placed in a vacuum chamber. Polystyrene micro-beads (78462, Sigma-Aldrich, UK) were then positioned on the cantilevers using a micro-positioner. The masses and diameters of the beads were 188.6 ± 16.6 pg and 7 ± 0.2 μm, respectively. Random signals with 1 MHz bandwidth generated by a function generator (33500B, Agilent, USA) were applied to the PZT, resulting in an rms velocity input of 0.49 mm/s. The vibration velocities of the excited cantilevers were measured at $x_1 = L/5$, where the first four bending modes of the cantilever vibration are measurable, via a single-point laser Doppler vibrometer (Polytec, Germany). It should be noticed that the sensitivity of the wavenumber determined from the transfer function to experimental uncertainties depended on the measurement location, x_1.[13] For the current cantilever and measurement set-up, the sensitivity was small enough when the vibration measurement location was close to the base, and the location $x_1 = L/5$ was determined empirically. The vibration velocities at $x = 0$ were also measured using the amplitude of the signals entering the PZT. These two velocities were measured before and after positioning the beads (Fig. 2).[8]

As the cantilever becomes smaller or the viscous effects become larger, the fluid-structure interaction becomes more important in determining the vibration characteristics. Figure 3(a) shows the viscosity effects of the surrounding fluid on the wavenumber of the flexural vibration for the fabricated (thin 1, 150 × 10 × 0.20 μm, 0.70 ± 0.20 ng) and commercial (thick, 458 × 51 × 2.0 μm, 109 ± 58 ng) cantilevers. As fluid viscosity increased, the wavenumber increased, suggesting that the wave propagation speed along the cantilever decreased due to the interaction with the enclosing fluid. This change was more pronounced in thin 1 cantilever. In fact, the commercial cantilevers in air exhibited a shift in the wavenumber by less than 0.5%, whereas the wavenumbers of the thin cantilevers varied by more than 5% in the real component, showing a significant fluid-structure interaction. The imaginary wavenumber components, which are associated with the damped vibration, also showed significant increases as the fluid viscosity increased.

The fluid-structure interaction must be analyzed prior to the identification of an attached mass and its position. Figure 3(b) shows the measured transfer functions when thin 1 cantilever was surrounded by air at different pressures. The predicted behaviors showed excellent agreement with the measured ones. With increasing air pressure, the measured resonant frequency and magnitude decreased due to inertial loading. This behavior was observed across the entire frequency range rather than only at frequencies close to the natural modes. Therefore, the transfer function (both magnitude and phase) and the wavenumber showed important information over a wide range of frequencies which contrast with the shift in the natural frequencies as used in most of the studies. This is a definite advantage of this method.

To estimate the influence of pressure on the fluid-structure interaction, the differences in the wavenumbers between given and reference pressures were measured. Although the wavenumbers in a vacuum are usually required for comparison, the wavenumbers at atmospheric pressure were used in this study. Figures 3(c) and 3(d) show the measured wavenumber deviations at different air pressures and

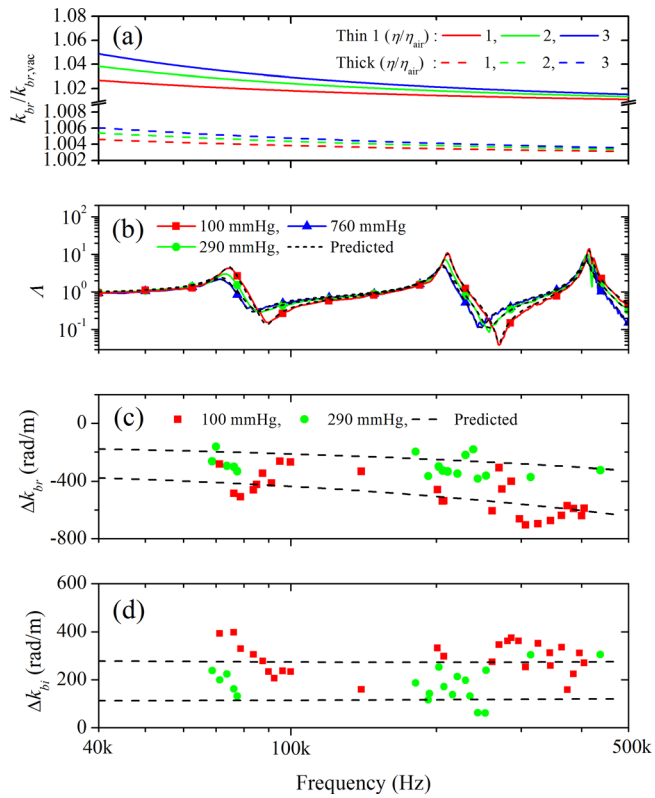

FIG. 3. (a) Wavenumbers ($\hat{k}_b = k_{br} - ik_{bi}$) for vibrations of the fabricated (thin 1) and commercial (thick) cantilevers as a function of frequency at several ratios of fluid viscosity. The dimensionless wavenumber determines the effects of the fluid-structure interaction on the cantilevers. (b) Transfer function of thin 1 cantilevers under the fluid-structure interaction in air (760 mmHg, 290 mmHg, and 100 mmHg). (c) Real part and (d) imaginary part of the difference between the wavenumbers at various pressures and the wavenumber at atmospheric pressure ($\Delta\hat{k}_b = \hat{k}_{b,fluid} - \hat{k}_{b,air(760mmHg)}$).

those predicted by Eq. (5) and the fluid properties reported in the literatures.[15,16] The deviations were almost constant across the measured frequency range and showed excellent agreement with the predictions, demonstrating that the transfer function measurements were in good agreement with the theoretical values even at higher resolution. It was also observed that the wavenumber decreased with decreasing air pressure, meaning that wave propagation along the cantilever increased.

After identifying the fluid-structure interaction of the bare cantilevers, beads were attached at several locations along the cantilevers. Figure 4(a) shows the measured and predicted transfer functions for different numbers of beads. The measured resonant frequencies decreased with number of attached beads. From the vibration responses, the equivalent mass was computed (Fig. 4(b)). The bead attachments increased the equivalent mass with a cyclic, frequency-dependent variation.

To determine the exact position of the beads, the *PI* was obtained using Eq. (8) (Fig. 4(c)). The optically measured and predicted bead positions are shown in Table I, and they have relative differences of 0.4%–10.1%. After determining the position of the beads, the mass of the beads was found (Fig. 4(d)). The measured bead mass changed with the frequency, but its variation was small. The predicted mass was in agreement with the measured one within one standard deviation, and the relative differences between the two values were observed to be 3.1%–8.5%. If the fluid-structure interaction is neglected, the difference increases up to 28.8%–69.6%. The maximum measured difference for one bead attachment was ~16 pg, where the mass ratio of the beads to the cantilever was 12%. The currently proposed method can provide quite accurate mass detection considering that the smallest masses (LOD) that resonant sensors can detect are 381 and 146 pg when thin 2 ($242 \times 24 \times 0.20\ \mu$m, 2.8 ± 0.20 ng) and 3 ($146 \times 24 \times 0.20\ \mu$m, 1.7 ± 0.13 ng) cantilevers are used, respectively. These minimum masses are based on the fundamental frequency shifts under thermal-noise excitation, which has been a commonly used method.[17] The mass ratio was quite large compared to the previous methods. In fact, the maximum mass ratio of the beads to the cantilever was almost 20% in the present study, and the previous approaches utilizing the Rayleigh quotient and assuming unaffected vibration mode shapes would result in large inaccuracies at such mass ratios.

TABLE I. Identified position and mass of the beads attached to thin 2 and 3 cantilevers in atmospheric air for different positions and numbers of beads, along with the theoretical predictions.

Measured values			Predicted values (in air)	
No. of beads	x/L	Beads mass (pg)	x/L	Beads mass (pg)
1	0.40	189 ± 17	0.36	183 ± 8
2	0.39	377 ± 33	0.36	365 ± 19
3	0.39	566 ± 50	0.36	593 ± 35
1	0.32	189 ± 17	0.32	205 ± 3
1	0.55	189 ± 17	0.55	200 ± 4
1	0.65	189 ± 17	0.68	183 ± 7

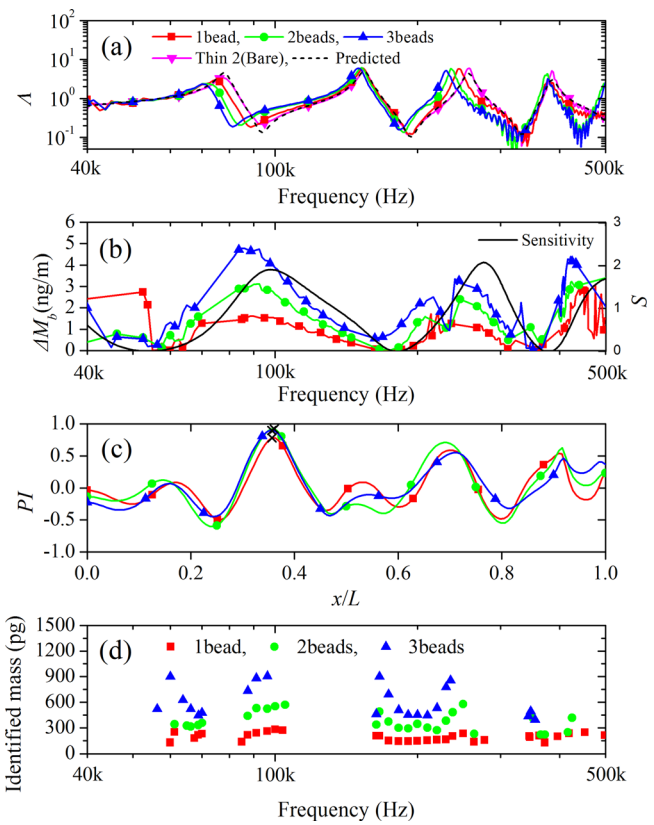

FIG. 4. (a) Transfer functions of thin 2 cantilever when the number of beads is increased. (b) Comparison of the sensitivity and ΔM_b calculated when the number of beads is increased for $x_a = 95\ \mu$m. (c) Position indicators (*PI*) calculated by using the correlation between ΔM_b and the sensitivity function for beads located at $x_a = 95\ \mu$m and (d) measured bead masses at different frequencies.

In conclusion, we have presented an experimental method to identify the position and the mass of beads attached to a nanoscale-thickness cantilever immersed in a viscous fluid by analyzing the effects of the fluid-structure interaction caused by the surrounding fluid on the cantilever vibration. The interaction was identified by measuring the change in the wavenumber due to the fluid for a cantilever without beads. Based on this acquired information, the position and mass of the beads were determined by measuring changes in the wave propagation due to the attached beads, and the predicted positions and masses agreed well with actual values. This method accurately determined both the fluid-structure interaction and the mass, even for heavy beads, by using wavenumber information at each frequency across a wide frequency range, unlike the previous studies that utilized only the natural frequencies and damping ratio. Moreover, this method can be quite independent of spurious peaks, a forest of peaks commonly observed in the frequency response when a cantilever is excited in liquid using a piezo-material, by using the transfer function between two vibration measurements.

This research was supported by Basic Science Research Program through the National Research Foundation of Korea (NRF) funded by the Ministry of Education, Science and Technology (2012R1A2A2A01012528 and 2012R1A2A2A 01004746).

[1]P. S. Waggoner and H. G. Craighead, Lab Chip **7**, 1238 (2007).
[2]R. Bashir, Adv. Drug Delivery Rev. **56**, 1565 (2004).
[3]Y. T. Yang, C. Callegari, X. L. Feng, K. L. Ekinci, and M. L. Roukes, Nano Lett. **6**, 583 (2006).
[4]S. Dohn, R. Sandberg, W. Svendsen, and A. Boisen, Appl. Phys. Lett. **86**, 233501 (2005).
[5]S. Dohn, W. Svendsen, A. Boisen, and O. Hansen, Rev. Sci. Instrum. **78**, 103303 (2007).
[6]S. Dohn, S. Schmid, F. Amiot, and A. Boisen, Appl. Phys. Lett. **97**, 044103 (2010).
[7]I. Stachiv, A. I. Fedorchenko, and Y.-L. Chen, Appl. Phys. Lett. **100**, 093110 (2012).
[8]D. Kim, S. Hong, J. Jang, and J. Park, Appl. Phys. Lett. **103**, 033108 (2013).
[9]J. E. Sader, J. Appl. Phys. **84**, 64 (1998).
[10]F. Fahy, *Sound and Structural Vibration: Radiation, Transmission and Response* (Academic Press, 1985).
[11]E. O. Tuck, J. Eng. Math. **3**, 29 (1969).
[12]L. D. Landau and E. M. Lifshitz, *Fluid Mechanics* (Pergamon Press, Oxford, 1987).
[13]J. Park, J. Sound. Vib. **288**, 57 (2005).
[14]S. Lee, S. Jeong, and J. Park, Proc. Inst. Mech. Eng., Part C. **228**, 2132 (2013).
[15]H. John Lienhard IV and H. John Lienhard V, *A Heat Transfer Textbook* (Phlogiston Press, Cambridge, Massachusetts, 2003).
[16]W. C. Hinds, *Aerosol Technology: Properties, Behavior, and Measurements of Airborne Particles* (Wiley, New York, 1999).
[17]A. Davila, J. Jang, A. Gupta, T. Walter, A. Aronson, and R. Bashir, Biosens. Bioelectron. **22**, 3028 (2007).